Modal Analysis Applied to Circular, Rectangular, and Coaxial Waveguides

D. J. Hoppe
Radio Frequency and Microwave Subsystems Section

This report summarizes recent developments in the analysis of various waveguide components and feedhorns using Modal Analysis (Mode Matching Method). A brief description of the theory is presented, and the important features of the method are pointed out. Specific examples in circular, rectangular, and coaxial waveguides are included, with comparisons between the theory and experimental measurements. Extensions to the methods are described.

I. Introduction

Modal Analysis has been shown to be a highly accurate and versatile method for analyzing a wide variety of waveguide devices [1]-[4]. The method is capable of accounting for multiple reflections within the device, stored energy at each discontinuity, and higher-order mode propagation if it occurs. Its high accuracy makes it useful for tolerance studies after a final design has been determined. This report compares computed and experimental results for the scattering parameters of three examples. One example is taken from each of the following waveguide types: rectangular waveguide, circular waveguide, and coaxial waveguide propagating the TE_{11} mode.

II. Theory

The theory described below is well known and is summarized in [1]. In applying the modal analysis method, the waveguide device is broken up into a series of sections that are joined by a step discontinuity as is shown in Fig. 1. For smooth changes in waveguide dimensions, the change is approximated by a large number of steps. At this point, the type of waveguide is arbitrary but the common area between the two guides must be identical to the cross-section of the smaller waveguide. This eliminates a class of offset connections but is usually not important for analyzing a practical device. In addition, for the circular waveguide and the coax, all guides are required to possess the same center line. This simplifies the analysis since only modes with one azimuthal variation need to be considered. Again, this is not restrictive for most practical applications. Next, the development of some of the important equations is presented. In Fig. 1, the fields to the left of the junction ($z < 0$) are represented as a sum of the normal modes of waveguide I.

$$\underline{E}_I = \sum_{m=1}^{M} (A_{Im}\, e^{-j\beta_m z} + B_{Im}\, e^{j\beta_m z})\underline{e}_{Im} \qquad (1)$$

$$\underline{H}_I = \sum_{m=1}^{M} (A_{Im}\, e^{-j\beta_m z} - B_{Im}\, e^{j\beta_m z})\underline{h}_{Im} \qquad (2)$$

Here M is chosen large enough for convergence, and $\underline{e}_{Im}$ and $\underline{h}_{Im}$ are the normalized vector functions for the mth mode. For example, in a circular waveguide, $m = 1 = TE_{11}$, $m = 2 = TM_{11}$, $m = 3 = TE_{12}$, etc. A_{Im} represents the magnitude of the forward traveling mth mode, and B_{Im} the magnitude of the reverse traveling mth mode.

The normalization of $\underline{e}_{Im}$ and $\underline{h}_{Im}$ is such that

$$\int_{S_I} (\underline{e}_{Im} \times \underline{h}_{Im}) \cdot ds = R_{mm} \tag{3}$$

and from the orthogonality of the waveguide mod

$$\int_{S_I} (\underline{e}_{Im} \times \underline{h}_{In}) \cdot ds = 0 \qquad m \neq n \tag{4}$$

Similarly, in region II

$$\underline{E}_{II} = \sum_{n=1}^{N} (A_{IIn}\, e^{j\beta_n z} + B_{IIn}\, e^{-j\beta_n z})\, \underline{e}_{IIn} \tag{5}$$

$$\underline{H}_{II} = \sum_{n=1}^{N} -(A_{IIn}\, e^{j\beta_n z} - B_{IIn} e^{-j\beta_n z})\, \underline{h}_{IIn} \tag{6}$$

where N is the number of modes chosen in region II. Relations analogous to Eqs. (3) and (4) hold for this region also.

Matching the electric and magnetic fields over the common aperture results in the following scattering matrix equation.

$$B = [S]\, A \tag{7}$$

$$B = \left[\frac{B_I}{B_{II}}\right] \tag{8}$$

$$A = \left[\frac{A_I}{A_{II}}\right] \tag{9}$$

and

$$[S] = \begin{bmatrix} [S_{11}] & [S_{12}] \\ [S_{21}] & [S_{22}] \end{bmatrix} \tag{10}$$

In Eqs. (8) and (9), B_I and B_{II} are vectors containing the reflected-mode amplitudes, while A_I and A_{II} contain the incident-mode amplitudes. The derivation of these equations is given in the Appendix.

For the normalized vectors, the power carried by the mth forward traveling mode is given by $|A_{Im}|^2$, and for the mth reverse traveling mode is $|B_{Im}|^2$.

Next, the matrices for a straight section of length L are needed. The solution is trivial, giving

$$[S_{11}] = [0] \tag{11}$$

$$[S_{12}] = [\gamma_{12}] \tag{12}$$

$$[S_{21}] = [\gamma_{21}] \tag{13}$$

$$[S_{22}] = [0] \tag{14}$$

where $[0]$ is the zero matrix and $[\gamma_{12}]$ and $[\gamma_{21}]$ are diagonal matrices with elements

$$\gamma_{21}(n,n) = \bar{e}^{\gamma_n L} = \gamma_{12}(n,n) \tag{15}$$

γ_n being the propagation constant for the nth mode and L being the section length.

This completes the summary of the required equations for each step in the analysis. Using these results, matrices for each step and each straight section in the device are determined and then combined using equations in [1]. At the completion of the analysis, the overall matrix is obtained, relating the normalized output vectors B_I and B_{II} at the ends of the device to the normalized input vectors A_I and A_{II}.

$$B_I = [S_{11}]\, A_I + [S_{12}]\, A_{II} \tag{16}$$

$$B_{II} = [S_{21}]\, A_I + [S_{22}]\, A_{II} \tag{17}$$

In many situations, a set of modes is incident only on the left end of a device and one wants to determine the reflected and transmitted modes. The user specifies the input mode vector A_I, $A_{II} = 0$, and Eqs. (16) and (17) become

$$B_I = [S_{11}]\, A_I \tag{18}$$

$$B_{II} = [S_{21}]\, A_I \tag{19}$$

III. Results

Computer programs [5] have been written to carry out the above calculations for rectangular, circular, and coaxial waveguides. For the junctions involved, the integrals of Eq. (A-6) can be carried out in closed form, which greatly simplifies the programming. Three examples, one in each waveguide type, are used to demonstrate the excellent agreement between theory and experiment. All of the measurements were made using an HP 8510 network analyzer and a full two-port calibration.

The first example, shown in Fig. 2, is a circular waveguide transition. For the theoretical results, 25 modes were used in the input section. The number of modes used in subsequent sections is chosen by the program for optimum convergence [1]. The return loss measurements (Fig. 3a) are typically within 0.2 dB, except near the minimum reflection point at 8.25 GHz. Phase results (Fig. 3b) are also in close agreement, typically within a few degrees across the band. For nearly every observation point, the difference between theory and measurement is within the accuracy specification of the network analyzer. Slight inaccuracies in the waveguide dimensions and rounding of some of the corners can also account for the small disagreement that remains. Figure 4 illustrates the convergence of the solution at 8 GHz as the number of modes used in the input section is increased. From these plots, we see that the solution has stabilized once 20 or more modes are used in the input waveguide. The number of modes required for convergence depends on the particular device, but in general larger waveguides with respect to a wavelength and thin irises require that more modes be used in order to get the same accuracy.

A rectangular waveguide example is shown in Fig. 5 and both theoretical and experimental results are given in Fig. 6. The device is a WR125 to 0.8-inch square-to-WR125 transition that was fabricated for use in the ring resonator at 8.51 GHz. The device consists of nine waveguide sections. The figure shows that, as in the previous example, the theoretical and experimental results are in excellent agreement. Only slight discrepancies appear near the minimum reflection point. More modes may be needed to represent the field in this region, or else the 0.030-inch radius on all corners, which was not accounted for in the calculation, may have a stronger effect in this frequency band. For this example, modes with first index m less than or equal to 7 and second index n less than or equal to 6 were used in the input guide. As with the circular waveguide program, maximum mode indices in the following sections are chosen according to waveguide size and symmetry considerations.

The final example is the coaxial iris shown in Fig. 7, with theoretical and experimental return loss results shown in Fig. 8. The coaxial region is excited by a TE_{11} circular waveguide mode that excites only the higher-order coax modes with first index equal to 1; the normal TEM coax mode is not excited in this case. Measurements of the iris were made by calibrating in the circular waveguide and using the time domain gating features of the HP 8510 network analyzer to isolate the reflections from only the iris. The only other complication associated with the coax is that a transcendental equation must be solved for each mode in each section in order to determine a cutoff wavelength. This increases the computation time required to solve a coax problem compared to a similar circular or rectangular waveguide problem. As with the previous examples, the agreement between theory and experiment is good, particularly considering the errors introduced by using the time domain features of the HP 8510.

IV. Conclusion

Three representative examples have been given to demonstrate the accuracy of the modal analysis method. A large number of waveguide devices such as horns, corrugated waveguides, transitions, filters, and smooth tapers can be analyzed using these programs. In addition, several extensions have been made to the codes in order to allow for differing dielectric constants in the sections, making them useful for window design. For large smooth-wall or corrugated horns, the reflection at the aperture may be neglected, and the far-field pattern can be found from the propagating modes in the aperture. In addition, the important case of ring-loaded slots [6], which is a combination of the coaxial and circular program, has also been programmed, but no experimental results are presently available.

Acknowledgments

The author would like to acknowledge the assistance of Dr. Farzin Manshadi in the development of the rectangular waveguide code, and Phil Stanton for providing the experimental data for the coaxial waveguide example.

References

[1] G. L. James, "Analysis and Design of TE_{11} to HE_{11} Corrugated Cylindrical Waveguide Mode Converters," *IEEE Trans. Microwave Theory Tech.*, vol. MTT-29, pp. 1059–1066, October 1981.

[2] E. Huhn and V. Hombach, "Computer-Aided Analysis of Corrugated Horns with Axial or Ring-Loaded Slots," *IEE Conf. Publ. 219 (ICAP 83) Part 1*, pp. 127–131, 1983.

[3] G. L. James, "Admittance of Irises in Coaxial and Circular Waveguides for TE_{11}-Mode Excitation," *IEEE Trans. Microwave Theory Tech.*, vol. MTT-35, pp. 430–434, April 1987.

[4] H. Patzelt and F. Arndt, "Double-Plane Steps in Rectangular Waveguides and Their Application for Transformers, Irises, and Filters," *IEEE Trans. Microwave Theory Tech.*, vol. MTT-30, pp. 771–776, May 1982.

[5] D. Hoppe, "Scattering Matrix Program for Circular Waveguide Junctions," in *Cosmic Software Catalog*, 1987 edition, NASA-CR-179669, NTO-17245, Georgia: NASA's Computer Software Management and Information Center, 1987.

[6] G. L. James and B. M. Thomas, "TE_{11} to HE_{11} Cylindrical Waveguide Mode Converters Using Ring-Loaded Slots," *IEEE Trans. Microwave Theory Tech.*, vol. MTT-30, pp. 278–285, March 1982.

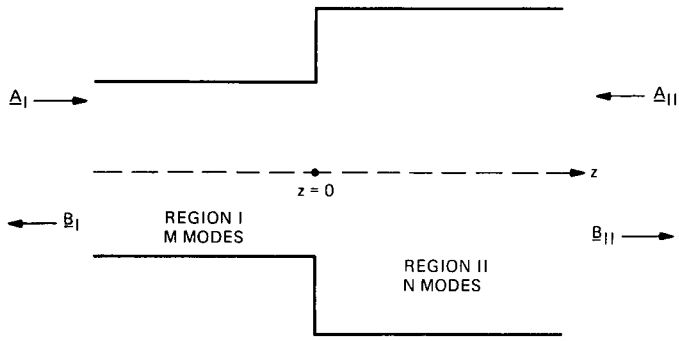

Fig. 1. Parameters for a single junction.

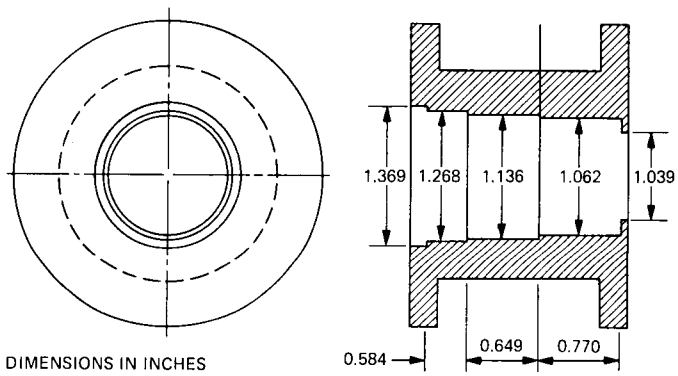

Fig. 2. Circular waveguide example.

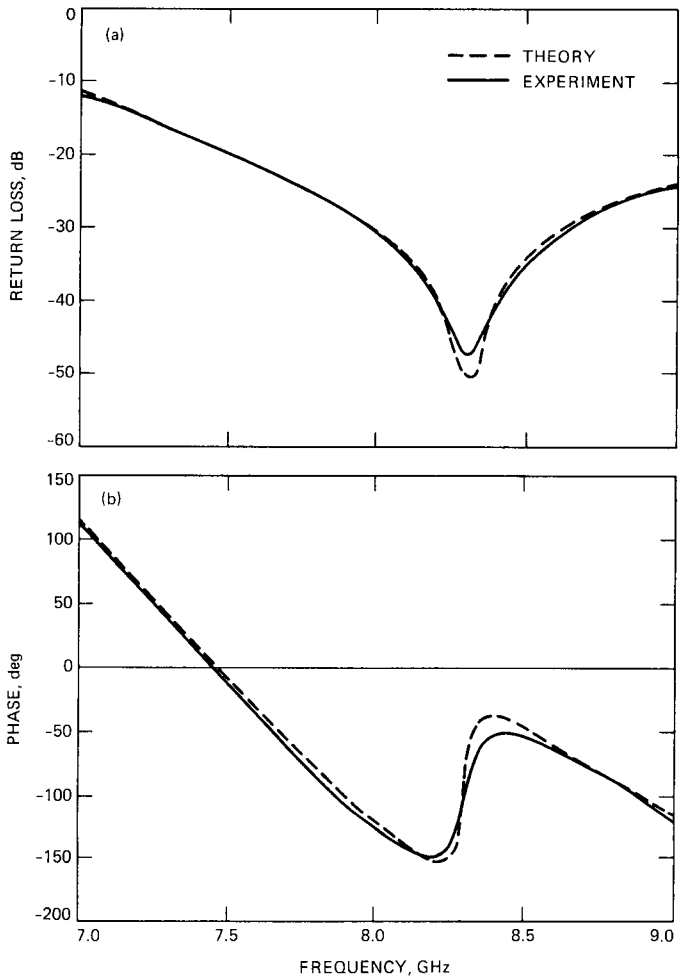

Fig. 3. Circular waveguide results: (a) return loss and (b) phase.

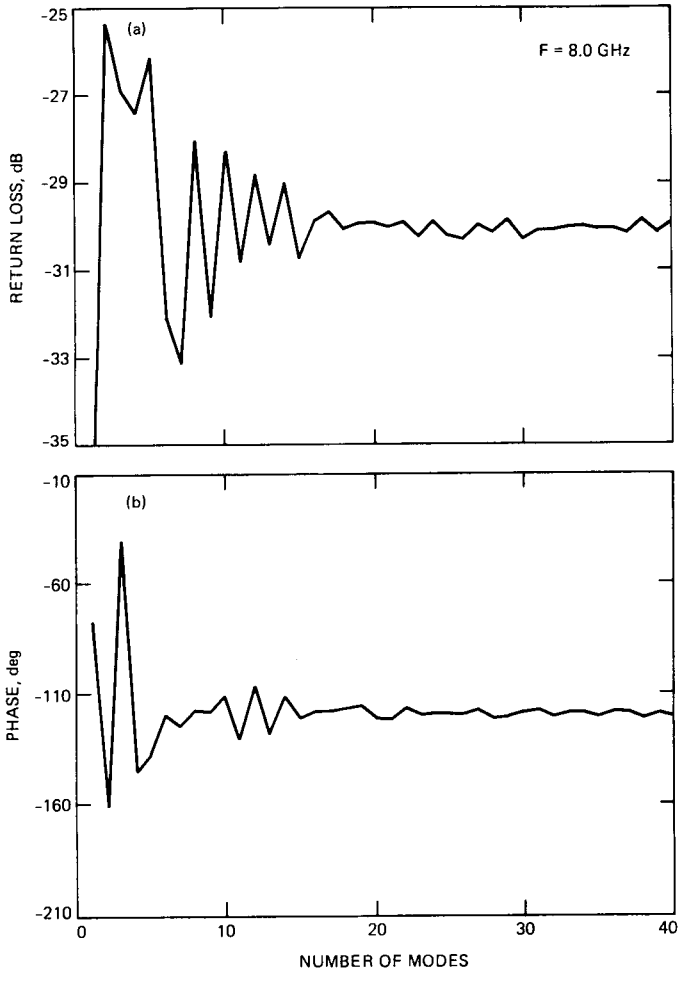

Fig. 4. Convergence for circular waveguide example: (a) return loss and (b) phase.

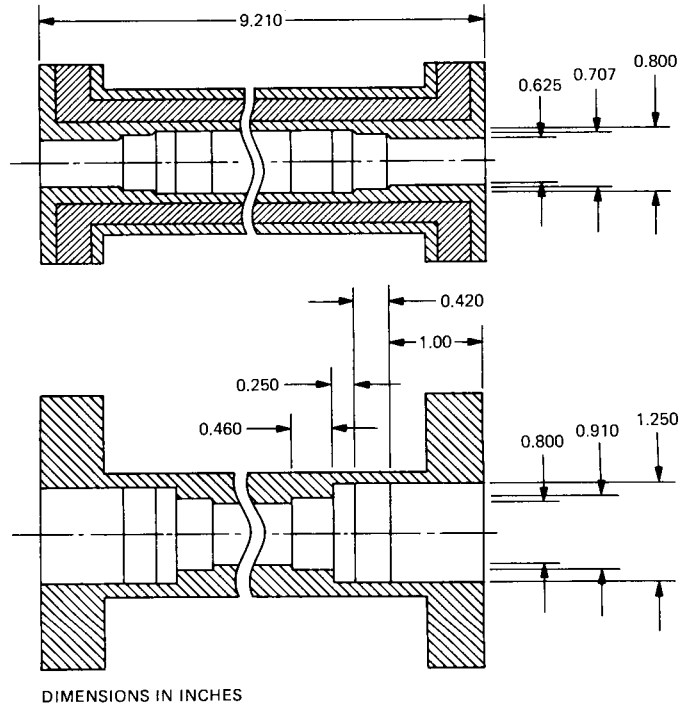

Fig. 5. Rectangular waveguide example.

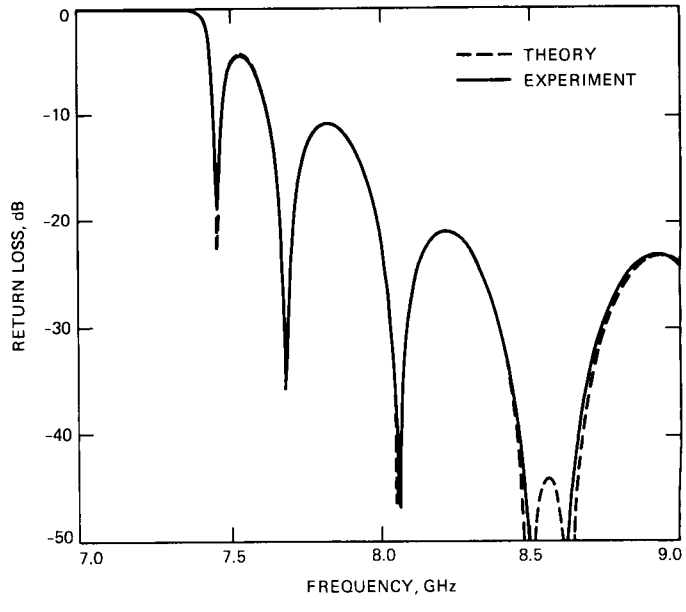

Fig. 6. Rectangular waveguide return loss results.

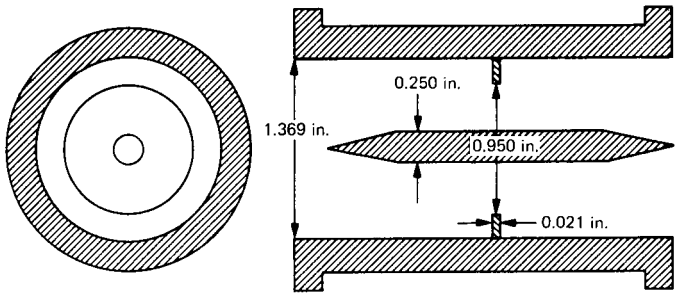

Fig. 7. Coaxial waveguide example.

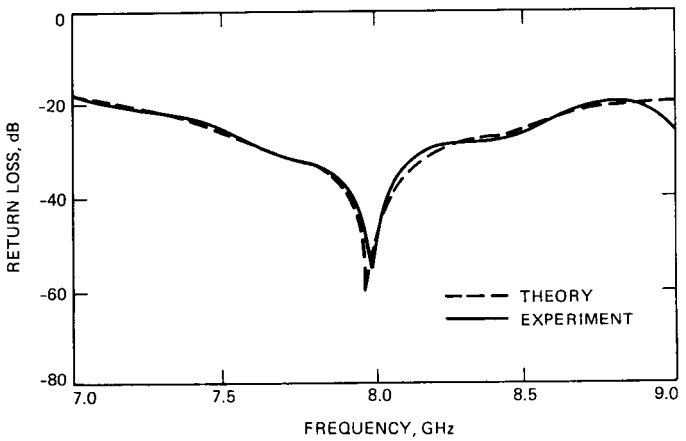

Fig. 8. Coaxial waveguide return loss results.

Appendix

Derivation of the Waveguide Scattering Matrix Equation

To derive Eq. (10), the electric fields inside the common aperture between the two regions are matched.

$$\underline{E}_I = \underline{E}_{II} \text{ inside } S_I \tag{A-1}$$

$$\underline{E}_I \times \underline{h}_{IIn} = \underline{E}_{II} \times \underline{h}_{IIn} \text{ inside } S_I \tag{A-2}$$

$$\int_{S_I} (\underline{E}_I \times \underline{h}_{IIn}) \cdot ds = \int_{S_I} (\underline{E}_{II} \times \underline{h}_{IIn}) \cdot ds \tag{A-3}$$

Since $E = 0$ on the conductor making up the surface $S_{II} - S_I$, the integral on the right-hand side of Eq. (A-3) may be extended over S_{II}.

$$\int_{S_I} (\underline{E}_I \times \underline{h}_{IIn}) \cdot ds = \int_{S_{II}} (\underline{E}_{II} \times \underline{h}_{IIn}) \cdot ds \tag{A-4}$$

Using the properties in Eqs. (1)–(6) the following is obtained:

$$\sum_{m=1}^{M} (A_{Im} + B_{Im}) P_{mn} = (A_{IIn} + B_{IIn}) Q_{nn} \tag{A-5}$$

where

$$P_{mn} = \int_{S_I} (\underline{e}_{Im} \times \underline{h}_{IIn}) \cdot ds \tag{A-6}$$

and

$$Q_{nn} = \int_{S_{II}} (\underline{e}_{IIn} \times \underline{h}_{IIn}) \cdot ds \tag{A-7}$$

The other boundary condition needed is

$$\underline{H}_I = \underline{H}_{II} \text{ within } S_I \tag{A-8}$$

Following a similar line of reasoning

$$\int_{S_I} (\underline{e}_{Im} \times \underline{H}_I) \cdot ds = \int_{S_I} (\underline{e}_{Im} \times \underline{H}_{II}) \cdot ds \tag{A-9}$$

giving

$$R_{mm}(A_{Im} - B_{Im}) = \sum_{n=1}^{N} P_{mn}(B_{IIn} - A_{IIn}) \tag{A-10}$$

$$R_{mm} = \int_{S_I} (\underline{e}_{Im} \times \underline{h}_{Im}) \cdot ds$$

Equations (A-5) and (A-10) may be recast into a more compact matrix form, giving

$$[P]\,(A_I + B_I) = [Q]\,(A_{II} + B_{II}) \tag{A-11}$$

$$[R]\,(A_I - B_I) = [P]^T\,(B_{II} - A_{II}) \tag{A-12}$$

Here $[P]^T$ is the transpose of the matrix $[P]$, and $[R]$ is an $m \times m$ diagonal matrix, and $[Q]$ is an $n \times n$ diagonal matrix.

Next, Eq. (A-12) is converted into a scattering matrix format relating the normalized output vectors B_I and B_{II} to the normalized input vectors A_I and A_{II}.

The submatrices $[S_{11}]$, $[S_{12}]$, $[S_{21}]$, and $[S_{22}]$ are derived from the $[P]$, $[P]^T$ $[R]$, and $[Q]$ matrices by simple matrix math and Eqs. (A-11) and (A-12).

$$[S_{11}] = [\sqrt{R}]\,([R] + [P]^T\,[P])^{-1}\,([R] - [P]^T\,[P])\,[\sqrt{R}]^{-1} \tag{A-13}$$

$$[S_{12}] = 2[\sqrt{R}]\,([R] + [P]^T\,[P])\,[P]^T\,[\sqrt{Q}]^{-1} \tag{A-14}$$

$$[S_{21}] = 2[\sqrt{Q}]\,([Q] + [P]\,[P]^T)\,[P]\,[\sqrt{R}]^{-1} \tag{A-15}$$

$$[S_{22}] = [Q]\,([Q] + [P]\,[P]^T)^{-1}\,([Q] - [P]\,[P]^T)\,[\sqrt{Q}]^{-1} \tag{A-16}$$

In these equations, $[I]$ represents the unit matrix and $[\sqrt{R}]\,[\sqrt{R}] = [R]$, and $[\sqrt{Q}]\,[\sqrt{Q}] = [\sqrt{Q}]$ are from Eqs. (3) and (7). These factors form the normalization of the vectors A and B. This completes the solution for the junction between the two different waveguides.